51st AIAA Aerospace Sciences Meeting including the New Horizons Forum and Aerospace Exposition
07 - 10 January 2013, Grapevine (Dallas/Ft. Worth Region), Texas

AIAA 2013-0283

Aerodynamic Shape Optimization of a Blended-Wing-Body Aircraft

Zhoujie Lyu*
Joaquim R. R. A. Martins†
Department of Aerospace Engineering, University of Michigan, Ann Arbor, MI

This paper presents aerodynamic shape optimization results for a 800-passenger blended-wing-body aircraft. A gradient-based optimizer and a parallel structured multiblock CFD solver are used. The derivatives are computed with an adjoint method, allowing optimization with respect to a large number of design variables. The aerodynamic shape optimization uses 807 shape and planform design variables to explore the design space. The objective function is the drag coefficient at a cruise condition. Both the lift and the root bending moment are constrained. The improvement due to the addition of planform variables is investigated. In addition, trim and stability constraints are considered in some of the optimization studies. We achieved an optimized blended-wing-body aircraft that satisfies both trim and static margin constraints, while minimizing the drag coefficient.

I. Introduction

With increasing environmental concerns and the rise in fuel prices, the aviation industry is facing a critical point where more fuel efficient aircraft options are needed in the near future. Several evolutionary advancements in aircraft wing design [1, 2], turbofan engine technology [3], and airline operations [4, 5] enable moderate reductions in fuel burn. However, a revolutionary step is needed to further reduce airline emissions. One possible step would be to develop unconventional aircraft configurations such as the blended-wing-body (BWB) aircraft.

The BWB is an unconventional aircraft configuration characterized by an enlarged and airfoil-shaped centerbody integrating with payloads, propulsion, and control surfaces. As discussed by several authors [6, 7, 8], the lift-generating centerbody section allows for higher aerodynamic efficiency compared to conventional aircraft. Additionally, the centerbody shields the ground from the engin noise, since they are mounted on top of the aircraft. The unique planform shape provides opportunities as well as challenges for advanced propulsion integrations, structural design, and stability and controls.

The concept of the BWB was not conceived until the 1980s. However, there were a number of designs throughout the aviation history that resembled the BWB configuration. The first aircraft to feature a blended wing and fuselage design was the Stout Batwing in 1918 [9]. The Junkers G.38 [10, 11] in 1929 was the first BWB design used for commercial purposes. Several military flying wings, such as Horten Ho 229, YB-49, and Northrop Grumman B-2, were also developed. Recently, two research BWB testbeds were built: a 6% scaled BWB built at Stanford University in 1995, as well as an 8.5% scaled NASA-Boeing X-48B and modified X-48C that are currently undergoing test flights. [12].

Several research projects have investigated BWB designs for more than two decades. When NASA began its preliminary study on future subsonic transport aircraft in 1988, the BWB was one of the proposed and evaluated aircraft [13, 14]. An 800-passenger BWB with a 7000 nautical mile range was studied both computationally and experimentally [15, 16, 17, 6, 18, 19, 12]. The MIT/Cambridge Silent Aircraft Initiative (SAI) studied the BWB configuration with a focus on noise reduction [20, 21, 22, 23]. The goal of this project was to achieve an aircraft design with 2030 technology level to feature a significant lower noise signature around the airport. A low-noise design of a 215-passenger BWB with a 5000 nautical mile range was proposed. The French national research project (AVECA), a collaboration between Airbus and ONERA, studied a low capacity BWB configuration [24, 25]. The New Aircraft Concepts Research (NACRE), also led by Airbus, studied winglet design for the BWB configuration [24].

*PhD Candidate, AIAA Student Member
†Associate Professor, AIAA Associate Fellow

The Very Efficient Large Aircraft (VELA) project in Europe studied a number of BWB configurations with different sweep angles [26, 27]. TsAGI, in collaboration with Airbus and Boeing, designed a 750-passenger BWB with a 7400 nautical mile range [28, 29, 30]. The Multidisciplinary Optimisation Of a Blended-Wing-Body (MOB) project is a collaboration between academia and industry in Europe [31, 32, 33, 34, 35]. RANS-based inverse design [36, 37] and Euler shape optimization [8] of the BWB were investigated in this project.

Through the above mentioned projects and other research [38, 39, 40, 41], the aerodynamic advantages of the BWB configuration have been widely studied. The blended-wing-body shape translates into significantly reductions in nearly all drag categories, and the explanation for these reductions can be summarized as follows:

- All-lifting design with low wing loading and desirable spanwise lift distribution — reduces lift-induced drag
- Lower wetted area compared to conventional aircraft — reduces skin friction drag
- Smooth and blended wing-centerbody junction — reduces interference drag
- Better area ruling — reduces wave drag
- Airfoil-shaped fuselage with a more streamlined aft body — reduces pressure drag

Despite its various aerodynamic benefits, the unique shape of the BWB configuration also brings challenges to the design process. The complex shape of the BWB may cause difficulties during manufacturing using composite materials. The chordwise lift distribution on the centerbody needs to be carefully designed to maintain trim and positive static margin. The thick airfoil shape of the centerbody makes it a challenge for the BWB to achieve low drag and generate sufficient lift at a reasonable deck angle. Trim and static margin are particularly critical for the BWB configurations due to the absence of conventional empennage. In this paper, we extend previous studies by using high-fidelity computational fluid dynamics (CFD) and numerical optimization tools to optimize the shape and planform of the BWB configuration while taking trim and stability into consideration. We use an efficient discrete adjoint implementation to the Euler solver [42] and a robust mesh perturbation method [43] that enable us to explore the design space using hundreds of geometric shape variables. We perform aerodynamic shape optimization with more than 800 design variables to obtain an optimized BWB design that is both trimmed and longitudinally stable.

The paper is organized as follows. The numerical tools used in this work are described in Section II. The problem formulation and the baseline geometry are shown in Section III. Finally, the results from the aerodynamic shape and planform optimization are discussed in Section IV.

II. Methodology

This section describes the numerical tools used in the aerodynamic shape optimization of the BWB aircraft. These tools are components of the MDO for aircraft configurations with high fidelity (MACH) framework [44]. An efficient geometric parametrization is used to allow manipulation of the aircraft shape and planform. The corresponding CFD volume mesh is then perturbed to match the modified geometry. We use a multiblock CFD solver in Euler mode to evaluate the aerodynamic performance. The derivatives for the optimization are computed with an adjoint method. Finally, a gradient-based optimizer is used to search the design space.

A. Geometric Parametrization

The choice of parametrization is not unique for aerodynamic shape optimization. There are several different geometric parametrizations such as basis vector, domain element, polynomial, spline, CAD, and free-form deformation (FFD). The geometric parametrization tool used in this work is developed by Kenway *et al.* [43, 44]. This approach utilizes the FFD proposed by Sederberg and Parry [45]. The FFD volume parametrizes the geometry changes rather than the geometry itself, resulting in an efficient and compact set of geometry design variables and complex geometrical manipulations. Any geometry may be embedded within the volume by performing a Newton search to map the parameter space to physical space. All the geometric changes are performed on the outer bound box of the FFD volume. Modification of the FFD volume indirectly changes the objects embedded in the volume. One important assumption of the FFD approach is that the geometry has constant topology throughout the optimization process, and this is usually the case for aerodynamic shape optimization. In addition, since the FFD volumes are constructed with tri-variate B-splines, the derivative of any point inside the volume can be computed analytically, which is crucial for aerodynamic shape optimization with respect to large number of design variables. The efficient computation of

geometric derivatives allow us to use more shape variables as compared to previous studies. Figure 1 shows the FFD volume and geometric control points for the BWB aerodynamic shape optimization. 800 shape control points are spread in a 20 by 20 grid on the upper and lower surfaces of the FFD volume.

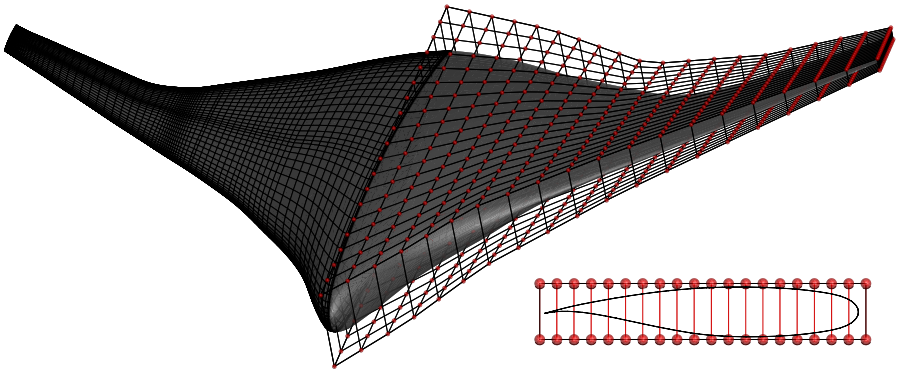

Figure 1. The BWB mesh (left), FFD volume and 800 shape control points (right)

B. Mesh Perturbation

While FFD volumes handle the modifications of the geometry, the mesh for CFD analysis also needs to be altered to match the modified geometry. The parallel mesh perturbation scheme used in this work, developed by Kenway *et al.* [43], is a hybridization between algebraic methods and linear elasticity methods. The linear elasticity-based warping is used to manage large perturbations on a coarsened mesh, while the algebraic warping is applied to local changes in the fine mesh. Since the mesh warping is performed several hundred times during the optimization, it needs to be efficient and robust, while maintaining the quality of the mesh. This method results in a much lower computational cost compared to linear elasticity-based warping. The one-time setup time for the BWB mesh warping of size 1.3 million cells is 70 seconds on 64 processors; however, each mesh warping takes only a fraction of a second to compute during the optimization.

C. CFD Solver

The flow solver used is the Stanford University multiblock (SUmb) [46]. SUmb is a finite-volume, cell-centered multiblock solver for the compressible Euler, laminar Navier–Stokes, and RANS equations (steady, unsteady, and time-periodic). It also provides options for a variety of turbulence models with one, two, or four equations. The flow solver uses hybrid 5th-order Runge–Kutta (RK) and Newton–Krylov(NK) methods, while the adjoint solution uses preconditioned GMRES [44, 47, 48, 49]. To facilitate the gradient-based optimization process, an ADjoint approach for the Euler solver that combines the discrete adjoint method and automatic differentiation was developed for the flow solver [42, 50]. The ADjoint approach uses an automatic differentiation technique to compute partial derivatives in the adjoint formulation. The adjoint implementation allows us to compute gradients with respect to hundreds of design variables with a computational cost of less than one flow solution.

D. Optimization Algorithm

Due to the computational cost of the CFD solver, it is critical to choose an efficient optimization algorithm that requires a reasonably low number of function calls. Gradient-free methods, such as genetic algorithms, have a higher probability of getting close to the global minimum for cases with multiple local minima. However, slow convergence and a large number of function calls would make gradient-free aerodynamic shape optimization infeasible with current computational resources. Therefore, we use gradient-based optimizers combined with adjoint gradient evaluations to achieve an efficient optimization process. Figure 2 shows the comparison between gradient and non-gradient-based optimizers using the Rosenbrock function [51] as the objective function, converged to a relative error of 10^{-3}. For a large number of design variables, the use of gradient-based optimizers is advantageous. We use a Python-based optimization package, *pyOpt* [52], to interface with CFD and adjoint solvers. We choose a gradient-based

optimization algorithm, Sparse Nonlinear OPTimizer (SNOPT) [53], as the optimizer. SNOPT is a sequential quadratic programming (SQP) method, designed for large-scale nonlinear optimization problems with thousands of constraints and design variables. It uses a smooth augmented Lagrangian merit function and the Hessian of the Lagrangian is approximated using a limited-memory quasi-Newton method.

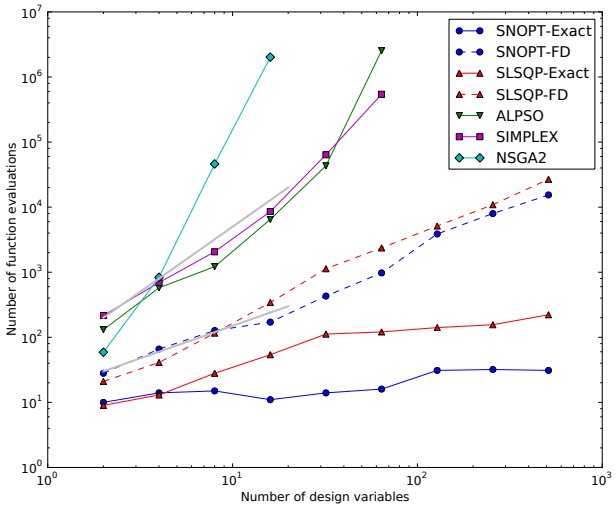

Figure 2. Number of function evaluations required to minimize the multidimensional the Rosenbrock objective function. SNOPT and SLSQP are gradient-based methods; ALPSO, Simplex and NSGA2 are gradient-free methods. The lower two lines correspond to the gradient-based methods used in conjunction with an efficient gradient computation.

III. Problem Formulation

Aerodynamic shape optimization of the BWB needs to be carefully formulated and constrained in order to achieve a physically feasible design. The following sections describe the baseline geometry, objective function, design variables, and constraints.

A. Baseline BWB Geometry

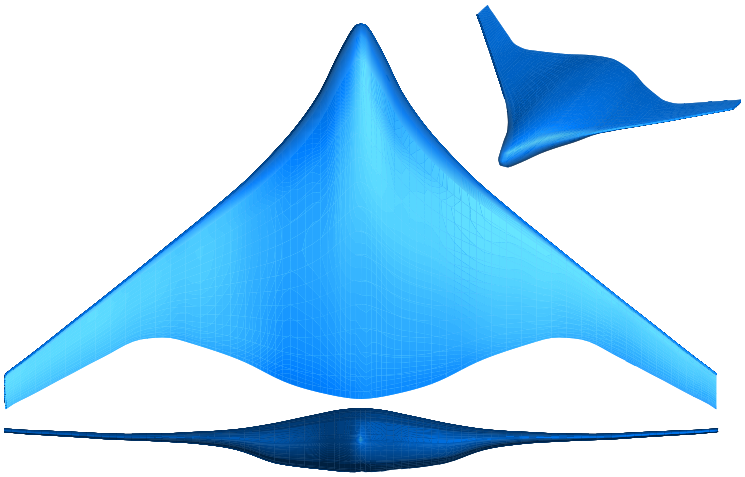

Figure 3. The baseline geometry of the 800-passenger BWB

The baseline geometry, shown in Figure 3, is an 800-passenger BWB aircraft with a 7000 nautical mile range. The planform shape is similar to the second generation Boeing BWB developed by Liebeck [6]. This geometry is divided into a centerbody section and an outer wing section. We use a modified NACA 0012 airfoil for the centerbody and a BAC 474 airfoil at the tip to provide an initial point for the optimization. The geometry is generated using *pyGeo* [43] with prescribed thickness-to-chord ratio, leading edge, and trailing edge without twist. The wing span is 274 ft, and the total length is 151 ft. The reference planform area is 7,762 ft^2. The trapezoidal aspect ratio is 9.7. The resulting wing loading of 106 lb/ft^2 is significantly lower than a conventional transonic transport aircraft by more than 30%. Its low wing loading provides a better handling quality at low speed and reduces the requirements for high lift devices. The center of gravity (CG) is set at 25% of the mean aerodynamic chord.

We optimize the aircraft at maximum cruise weight flying at Mach 0.8 and 30,000 ft attitude. Euler CFD analysis of the baseline BWB shows a drag coefficient of 0.02696 at its design lift coefficient of 0.440, indicating room for further improvement. The classic van Driest method with form-factor correction is used to compute the skin friction drag [54]. Table 1 summarizes the geometry and aerodynamic parameters of the baseline BWB.

Parameters	Baseline BWB	Parameters	Baseline BWB
Wing span	274 ft	Wing loading	106 lb/ft^2
Fuselage length	151 ft	CG location from nose	71.5 ft
Reference area	$7,762$ ft^2	Drag coefficient	0.02696
Trapezoidal aspect ratio	9.7	Lift coefficient	0.440
Mean aerodynamic chord	26.1 ft	Static margin	19.1%

Table 1. Summary of the baseline BWB

Structured multiblock grids of 1.3 million cells are created for the baseline geometries. This grid size is chosen such that it can accurately resolve the geometry and flow field, while incurring an acceptable computational cost. Each flow solution with Euler CFD solver is performed in about 60 seconds on 64 processors.

B. Objective Function

We choose drag coefficient as the objective function for the optimization under prescribed lift. The drag coefficient has two components: drag coefficient from the Euler solver, and the skin friction drag coefficient. The van Driest method is used to capture the missing skin friction drag from the Euler solver. Skin friction drag is particularly important for trade-off between wing span and wing area.

C. Design Variables

Primary design variables are the geometric shape variables distributed on the FFD volume. A total of 800 shape variables are scattered on the lower and upper surfaces of the FFD volume, as shown in Figure 1. The large number of shape variables provides more degrees of freedom for the optimizer to explore, and to fine-tune the sectional airfoil shape and thickness-to-chord ratio at each spanwise location. We use significantly more shape variables than in the previous studies in the literature. This is made possible by the implementation of an adjoint gradient calculation. We found that the cost of computing shape gradients is nearly independent of the number of shape variables.

The next set of design variables is the spanwise twist distribution. A total of 5 section twist design variables is used. The center of twist rotation is fixed at the reference axis, which is located at the quarter chord of each section. The twist variables provide a convenient way for the optimizer to minimize induced drag by adjusting the spanwise lift distribution, as well as to meet the root bending moment constraint.

Planform variables, such as span and sweep, are also considered in the optimization, and they contribute primarily to the reduction of induced drag and wave drag, respectively. The span design variable stretches the FFD volume in the spanwise direction. The sweep variable shears the FFD volume in chordwise direction. The planform variables can only be added to the optimization together with the bending moment constraint and the skin friction estimation, since the planform variation changes the structural weight and surface area significantly.

Auxiliary design variables are added to facilitate the formulation of the optimization problem. The angle-of-attack variable ensures that the lift coefficient constraint can be satisfied. We use an individual design feasible (IDF)

approach [55] to update the reference CG location (x_{CG}) and the mean aerodynamic chord (MAC). This requires the addition of a target variables, x^t_{CG} and MAC^t. Table 2 summarizes the design variables.

Design Variables	Count	Design Variables	Count
Airfoil Shape	800	Angle-of-attack	1
Twist	5	Target CG location	1
Span	1	Target MAC	1
Sweep	1	**Total**	**810**

Table 2. Summary of the design variables used in the BWB aerodynamic shape optimization problem

D. Constraints

As optimizers tend to explore any weakness in the numerical models, an optimization problem needs to be carefully constrained in order to yield a physically feasible design. Several geometric constraints are implemented. We impose thickness constraints near the leading edge (LE), trailing edge (TE), mid-chord, and centerbody to prevent the airfoil thickness from affecting low speed aerodynamic performance, to get a reasonable structural box depth, and to prevent the violation of the manufacturing constraints. These constraints also ensure sufficient height in the centerbody cabin and sufficient thickness at the LE and TE for the installation of high-lift devices such as slats and flaps. The volume of the centerbody is also constrained to meet the requirements for cabin and payload space. The wing volume constraints are also imposed to ensure sufficient space for fuel. In order to avoid generating non-physical kinked LE and TE, the shape variables located at the LE and TE are constrained so that each pair of shape variables can move only in opposite direction with equal magnitudes.

Due to the absence of a structural model, we use root bending moment as a surrogate for the structural weight trade-offs. The root bending moment is constrained to be equal or less than the baseline bending moment. With this constraint imposed, the optimized spanwise lift distribution tends less outboard loading instead of the elliptical distribution [56]. The bending constraint is necessary to capture the trade-offs between aerodynamic performance and structural weight.

In addition, the BWB has to be trimmed in cruise conditions without the need to deflect its control surfaces which would result in trim drag. Therefore, a trim constraint is added. There are several way to trim a flying wing: by unloading wing tips on a swept wing, by adding reflex to the airfoils at the trailing edge, and by adding anhedral to wing tips [57]. Our optimization problem has all the required degrees of freedom to explore the design space except for the anhedral wing tips. In addition, stability is a particularly important design aspect of the BWB configuration. With the absence of a conventional empennage, it is not immediately obvious whether a positive static margin can be achieved on a BWB aircraft. Therefore, we constrained the static margin to be greater than 5%. The static margin can be calculated as the ratio of the moment and lift derivatives [41].

$$K_n = -\frac{C_{M_\alpha}}{C_{L_\alpha}}, \tag{1}$$

We calculate C_{M_α} and C_{L_α} using finite differences with an angle-of-attack step size of 0.1 degree. The static margin constraint incurs an additional computational cost. For each iteration, one additional flow solution and two additional adjoint solutions are required. Both flow and adjoint solutions have to be converged more accurately than usual to obtain an accurate static margin gradient. This is particularly important for static margin gradients with respect to shape variables, since they have relatively small magnitudes compared to other gradients.

The IDF formulation requires two additional compatibility constraints for the CG location and MAC. Table 3 summarizes the constraints for the optimization problem.

IV. Aerodynamic Shape and Planform Optimization Results

The following sections discuss the results from performing a sequence of aerodynamic shape and planform optimizations. The baseline BWB geometry is used as the initial design. The optimizations are performed with an Euler solver and a friction drag estimation, as described in Section III. All cases are run on high performance computing

Constraints	Count	Constraints	Count
Lift coefficient	1	Trim	1
Thickness	99	Static margin	1
Internal volume	99	CG compatibility	1
LE, TE control points	40	MAC compatibility	1
Total	**243**		

Table 3. Summary of the constraints used in the BWB aerodynamic shape optimization problem

clusters in the Center for Advanced Computing at the University of Michigan [58]. Each computing node comprises two six-core 2.67 GHz Intel Xeon X5650 processors with 4 GB of RAM per core. All the nodes are interconnected with InfiniBand networking. A total of four cases are presented in this section.

Case 1: Baseline lift-constrained drag minimization with respect to shape variables and with geometric constraints
Case 2: Lift-constrained drag minimization with respect to shape variables, with geometric, root bending moment, and trim constraints
Case 3: Lift-constrained drag minimization with respect to shape and planform variables, with geometric, root bending moment, and trim constraints
Case 4: Lift-constrained drag minimization with respect to shape and planform variables, with geometric, root bending moment, trim, and static margin constraints

A. Case 1: baseline lift-constrained drag minimization with respect to shape variables and with geometric constraints

In order to validate our optimization formulation, we begin with a baseline optimization case with only geometric and lift constraints. The design variables are shape variables, twist, and angle-of-attack. Without any additional constraints, we expect to see an optimum elliptical lift distribution and weakened shocks. Since only one flow solution and two adjoint systems need to be solved, the problem requires less computational time than the other cases. The optimization is performed using 16 cores, and is converged in 34 hours with a total of 91 major optimization iterations. Figure 4 shows the pressure distribution, airfoil shape, and lift, thickness-to-chord ratio (t/c), twist distributions of the baseline and optimized BWB configurations. The aerodynamic coefficients of the baseline and optimized BWB are listed in Table 4. Figure 5 shows the convergence history of the feasibility, optimality, and merit function.

Coefficient	Baseline	Optimized	Difference
C_D	0.02696	0.02245	-16.7%
C_L	0.440	0.440	0.0%
$C_{M_{root}}$	0.2599	0.2731	+5.1%
$C_{M_{trim}}$	0.1938	0.2037	+5.1%

Table 4. Case 1: aerodynamic coefficients of the baseline and optimized BWB

The optimized BWB achieves an optimal elliptical spanwise lift distribution, mostly by varying the sectional twist distribution. Both root and tip of the wing are twisted down and the mid-span section is twisted up to match the elliptical lift. The airfoil shape of the centerbody is not significantly altered. Changes made to the shape of the centerbody are mainly to smooth out the pressure distribution. A large portion of lift is generated on the aft section of the centerbody because of the airfoil camber, resulting in a pitch down moment. The optimized BWB further increases the pitch down moment by 5.1%, indicating the need for a trim constraint.

A strong stock can be seen at the leading edge of the upper wing section on the baseline BWB. The shock transits into a compression wave toward the centerbody. The shock structure on the optimized BWB is significantly different. The pressure distribution on the upper surface is flattened compared to that of the baseline BWB. The strong shock at the leading edge is weakened and shifted to the mid-chord, reducing the wave drag. The drag coefficient is reduced by 45 counts or 16.7%. With the optimal lift distribution, lift is shifted toward the wing tip. We can see that the root

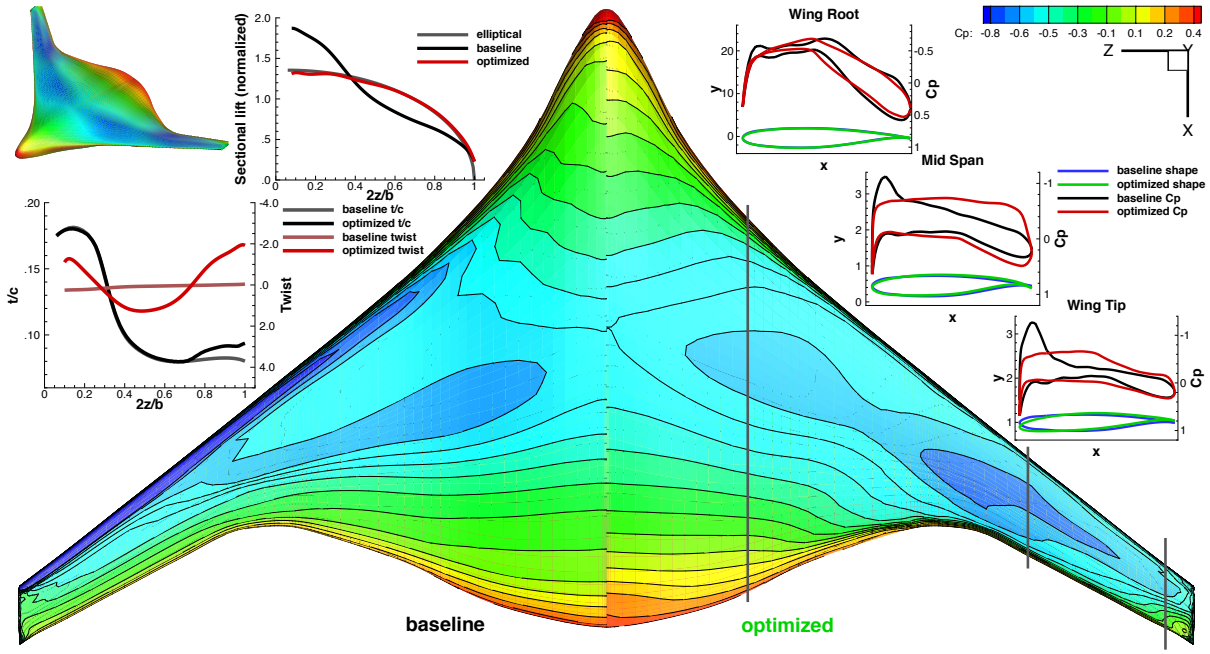

Figure 4. Case 1: the results of the baseline lift constrained drag minimization with shape variables and geometric constraints. Pressure contour, sectional C_p distribution, airfoil shape, and spanwise lift, t/c, twist distributions of the baseline design (left) and the optimized design (right) are shown.

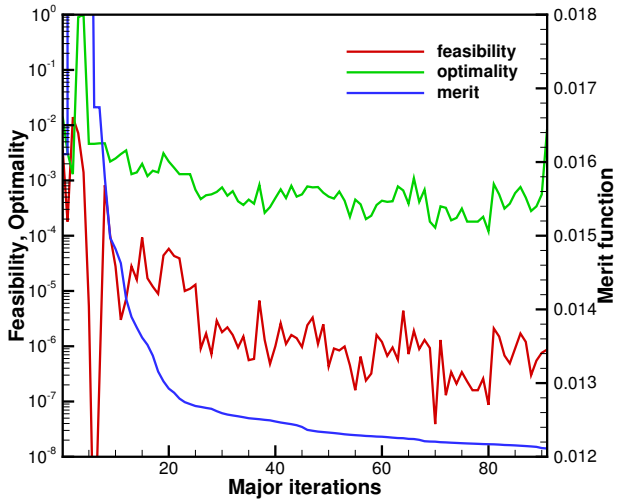

Figure 5. Case 1: SNOPT optimization convergence history of the feasibility, optimality, and merit function

bending moment increases by 5.1%, which indicates that a heavier structure would be required. Therefore, a root bending moment constraint is necessary to constrain the impact on structural weight.

This baseline optimization serves as a validation of the optimization formulation. We obtain an elliptical lift distribution and reduced shock strength on the upper surface. We can also conclude that additional constraints are needed to achieve a practical design.

B. Case 2: lift-constrained drag minimization with respect to shape variables, with geometric, root bending moment, and trim constraints

As discussed in the previous case, we need to capture the trade-offs between the aerodynamic performance, structural weight, and trim drag. Therefore, root bending moment and trim constraints are added. The root bending moment is constrained to be less than or equal to the initial bending moment. Two additional adjoint systems are needed to compute the gradient of those constraints. This optimization problem is converged in 72 hours using 16 cores, and requires a total of 321 iterations. Figure 6 shows the pressure distribution, airfoil shape, and lift, t/c, twist distributions of the baseline and optimized BWB configurations. Note that for the purpose of visualize the airfoil shape, x and y axes of the sectional airfoil plots are not of the same scale. Therefore, the sectional twist in these plots is not to scale. The aerodynamic coefficients of the baseline and optimized BWB are listed in Table 5. Figure 7 shows the convergence history of the feasibility, optimality, and merit function.

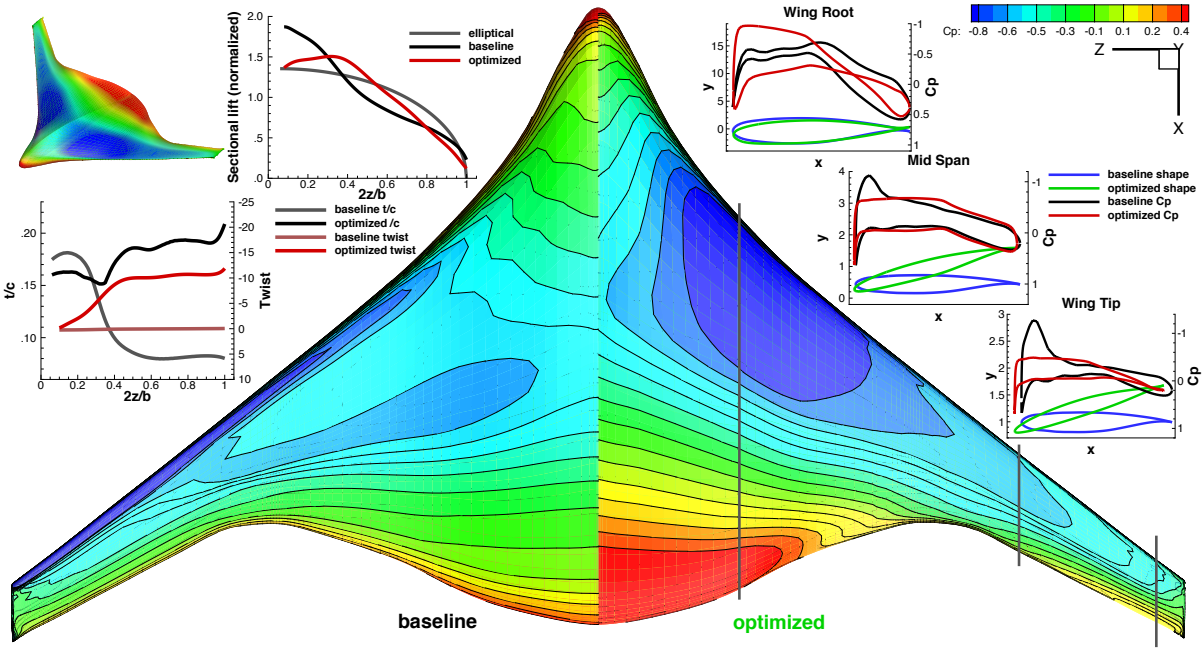

Figure 6. Case 2: the results of the lift constrained drag minimization with shape variables, geometric, root bending moment, and trim constraints. Pressure contour, sectional C_p distribution, airfoil shape, and spanwise lift, t/c, twist distributions of the baseline design (left) and the optimized design (right) are shown.

Coefficient	Baseline	Optimized	Difference
C_D	0.02696	0.02381	-11.7%
C_L	0.440	0.440	0.0%
$C_{M_{root}}$	0.2599	0.2599	0.0%
$C_{M_{trim}}$	0.1938	0.0	-100%

Table 5. Case 2: aerodynamic coefficients of the baseline and optimized BWB

With the addition of root bending moment constraint, the optimized spanwise lift distribution is no longer elliptical. The lift on the wing section decreases more linearly toward the wing tip. This departure from the elliptical lift distribution limits span efficiency and hinders improvements in induced drag. However, it benefits the structural weight and lateral control response for a flying wing [59, 60]. Two design features that lead to satisfaction of trim constraints on a trimmed flying wing are observed on the optimized BWB. The first is a reflex near the trailing edge of the optimized centerbody airfoil, resulting in a significant change to the chordwise lift distribution on the centerbody. All lift is generated at the forward section of the centerbody, while the aft centerbody has negative lift to trim the aircraft. As a result, the net lift on the centerbody is reduced, as shown on the lift distribution plot. The second feature

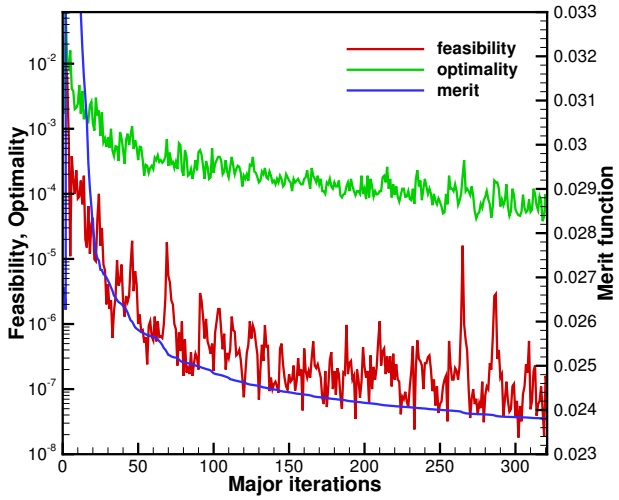

Figure 7. Case 2: SNOPT optimization convergence history of the feasibility, optimality, and merit function

is the unloaded wing tip. The optimized wing tip airfoil has washout and less lift than the baseline. The unloaded wing tips on a highly swept wing act as the horizontal tail to trim the aircraft.

Due to these constraints, optimized drag is reduced by 31 counts as compared to 45 counts in the previous case. This change is primarily due to a lower span efficiency and the presence of the reflex centerbody airfoil, which causes the lift induced drag and the trim drag to increase.

C. Case 3: lift-constrained drag minimization with respect to shape and planform variables, with geometric, root bending moment, and trim constraints

In this case, we seek the benefits of adding planform design variables to the optimization described in Case 2. By allowing changes to the span and sweep, we provide the optimizer with greater degrees of freedom and an efficient way of satisfying the trim constraints and reducing wave drag. This optimization problem is converged in 95 hours with 16 cores, and requires with a total of 426 iterations. The increased optimization time is mainly due to the increase in design space dimensionality. Figure 8 shows the pressure distribution, airfoil shape, and lift, t/c, twist distributions of the baseline and optimized BWB. The aerodynamic coefficients of the baseline and optimized BWB are listed in Table 6. Figure 9 shows the convergence history of the feasibility, optimality, and merit function.

Coefficient	Baseline	Optimized	Difference
C_D	0.02696	0.02338	-13.3%
C_L	0.440	0.440	0.0%
$C_{M_{root}}$	0.2599	0.2599	0.0%
$C_{M_{trim}}$	0.1938	0.0	-100%

Table 6. Case 3: aerodynamic coefficients of the baseline and optimized BWB

The sectional pressure distribution and pressure contour are relatively similar to those in the previous cases. The addition of planform variables does not significantly alter the pressure distribution. The optimized BWB also has a reflex centerbody and an unloaded wing tip to trim the aircraft. The span of the optimized BWB is approximately the same as the baseline, while the sweep angle of the wing increased significantly. The increase in sweep angle reduces wave drag and also helps to trim the aircraft by increasing the moment arm of the unloaded tips. The wing tip generates a higher amount of lift compared to the previous case. The amount of centerbody reflex is reduced. The optimizer finds that trim with sweep and twist is more effective, which results in lower trim and induced drag. The increase in span is limited because of the root bending moment constraint and skin friction drag penalty.

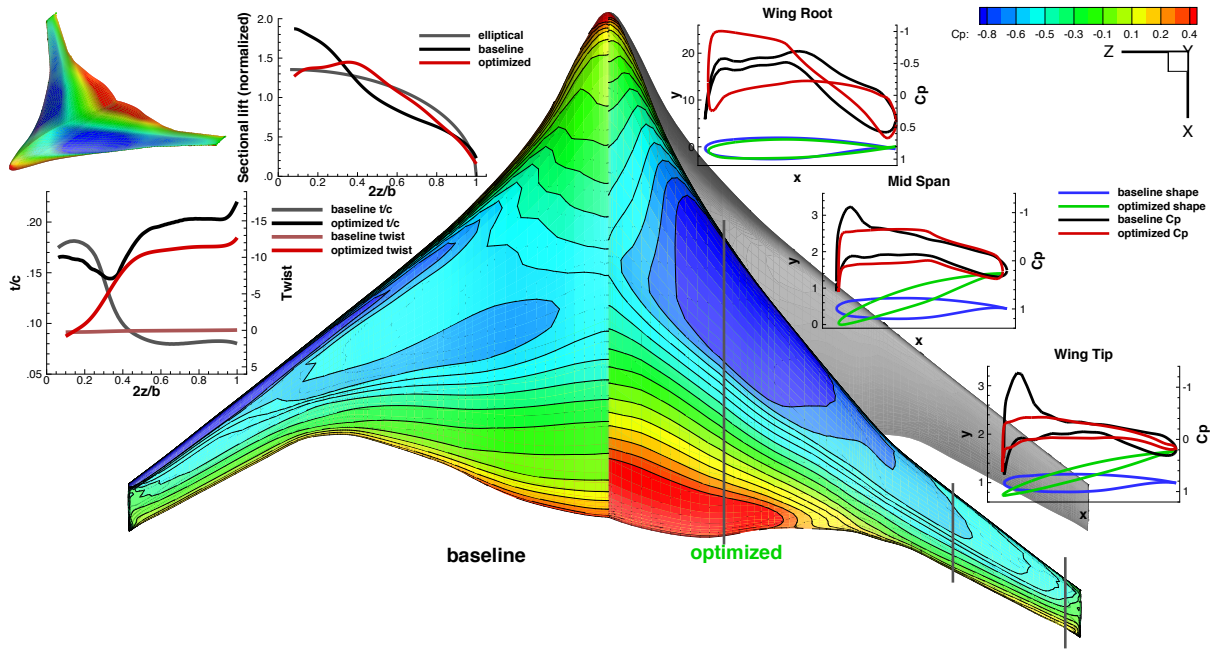

Figure 8. Case 3: the results of the lift constrained drag minimization with shape and planform variables, geometric, root bending moment, and trim constraints. Pressure contour, sectional C_p distribution, airfoil shape, and spanwise lift, t/c, twist distributions of the baseline design (left) and the optimized design (right) are shown.

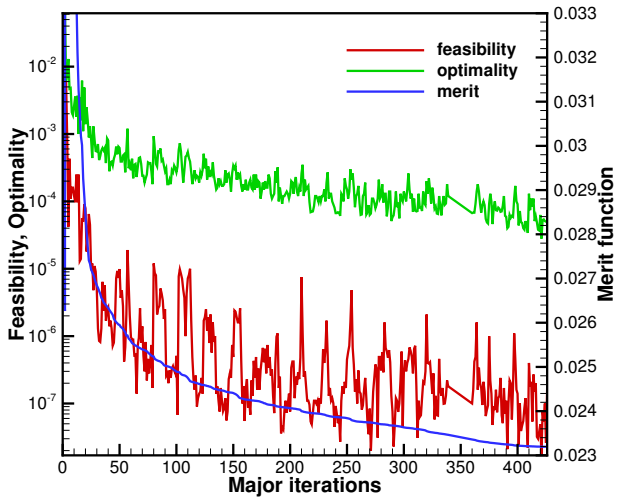

Figure 9. Case 3: SNOPT optimization convergence history of the feasibility, optimality, and merit function

D. Case 4: lift-constrained drag minimization with respect to shape and planform variables, with geometric, root bending moment, trim, and static margin constraints

The optimization setup for this case is similar to that of Case 3, with the exception of an additional static margin constraint. The goal of this case is to use numerical optimization to achieve an optimized longitudinally stable and trimmed configuration that would be otherwise difficult to design with a trial-and-error design process. The static margin is computed by performing finite difference of the lift and moment coefficients. We also added the payload location as a design variable, and this is represented by the CG location. The CG is allowed to move between 20% to 50% of the MAC.

This optimization problem is more computationally intensive than the previous cases for several reasons. Each iteration requires two flow solutions and six adjoint solutions in order to obtain the static margin and its gradient. The static margin gradient is a second order derivative, since it is the gradient of lift and moment coefficient gradients. Therefore, in order to achieve an accurate static margin gradient, both flow and adjoint solutions need to be converged to a higher tolerance (10^{-10}). Finite-differencing the lift and moment coefficients perturbs only the angle-of-attack. If a Newton-type iteration, such as the Newton–Kylov method, is used to solve the flow solution, the Maratos effect [61] may cause the Newton iteration to stall. We increase number of Runge–Kutta iteration before switching to the Newton-Krylov solver. A flow field solution reset is used as a fail-safe procedure if the solution stalls.

This optimization problem converged in 58 hours on 64 cores with a total of 138 iterations. Figure 10 shows the CG and neutral point (NP) locations, pressure distribution, airfoil shape, and lift, t/c, twist distributions of the baseline and optimized BWB configurations. The aerodynamic coefficients of the baseline and optimized BWB are listed in Table 7. Figure 11 shows the convergence history of the feasibility, optimality, and merit function.

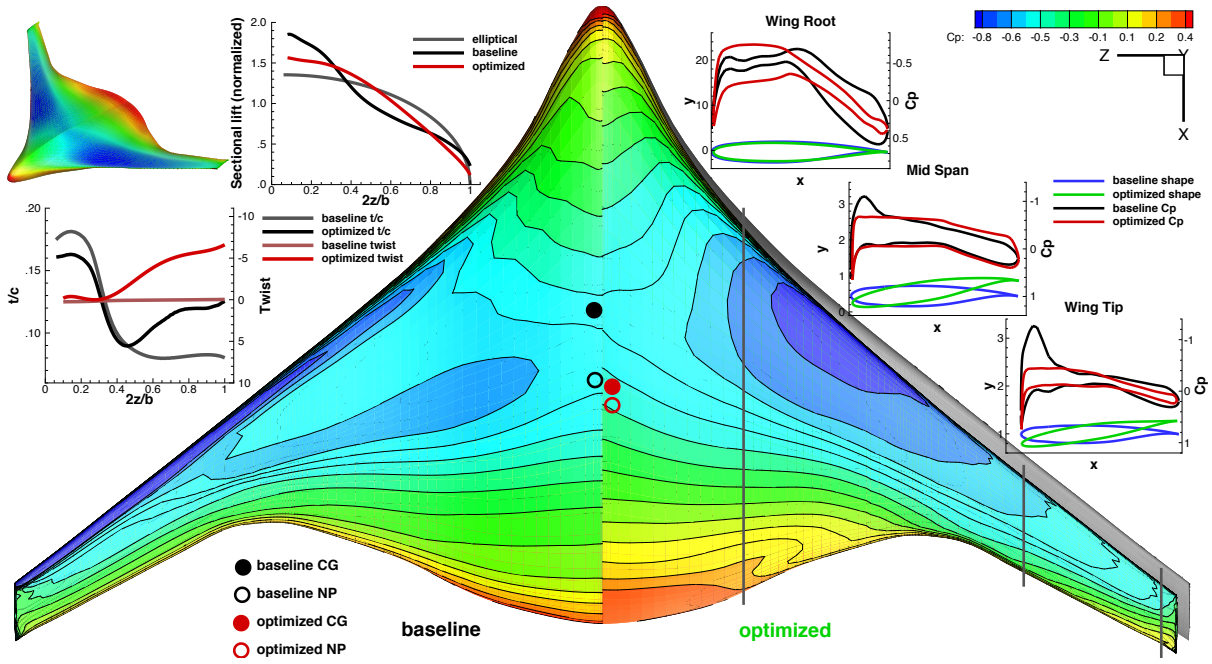

Figure 10. Case 4: the results of the lift constrained drag minimization with shape and planform variables, geometric, root bending moment, trim, and static margin constraints. CG and NP locations, pressure contour, sectional C_p distribution, airfoil shape, and spanwise lift, t/c, twist distributions of the baseline design (left) and the optimized design (right) are shown.

Coefficient	Baseline	Optimized	Difference
C_D	0.02696	0.02339	-13.2%
C_L	0.440	0.440	0.0%
$C_{M_{root}}$	0.2599	0.2599	0.0%
$C_{M_{trim}}$	0.1938	0.0	-100%
K_n	19.1%	5.0%	/

Table 7. Case 4: aerodynamic coefficients of the baseline and optimized BWB

Both static margin and trim constraints are sensitive to the CG location. Since a lower trim moment is required for an aft CG location, the trim constraint tends to move the CG backward by increasing CG design variable or by increasing the sweep angle. On the contrary, the CG location is also constrained by the static margin, since an aft CG location decreases the static margin. For a flying wing, location of the NP coincides with the aerodynamic center, the point about which the pitching moment coefficient does not vary with angle-of-attack. For a fixed planform, the

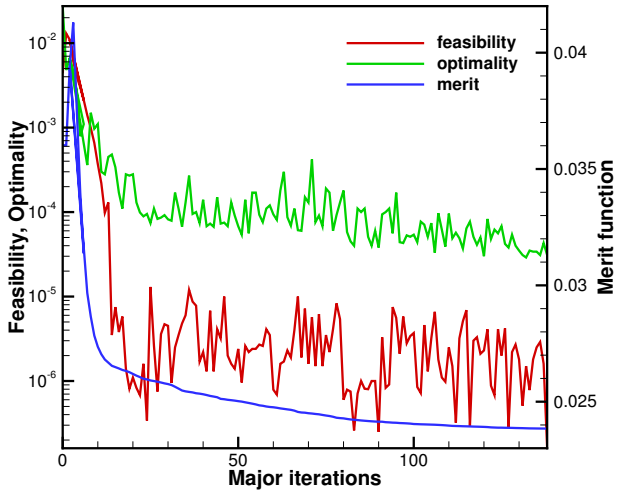

Figure 11. Case 4: SNOPT optimization convergence history of the feasibility, optimality, and merit function

aerodynamic center varies only slightly with the airfoil shape variables. The static margin constraint is most sensitive to the sweep angle. As sweep angle increases, both aerodynamic center and mean aerodynamic chord shift aft. However, the mean aerodynamic chord moves at a faster rate than the aerodynamic center. Thus, the static margin decreases for an increasing sweep. This effect can be seen from the optimization results. The sweep angle only increases slightly as compared to the previous case, which is constrained by the static margin. The static margin of the BWB is reduced from 19.1% in the baseline configuration to 5.0% in the optimized configuration. The CG moved from 25% of the MAC to 47%.

Because of the aft CG location than the previous cases, the trim constraint becomes less difficult to satisfy. We can see from the pressure distribution that the amount of reflex and down twist is reduced. Only aft centerbody has a reflex shape airfoil. The optimized BWB has better aerodynamic performance due to the relaxed CG location. It has a drag that is 36 counts lower than the baseline.

E. Summary of the Aerodynamic Shape and Planform Optimization Results

The four cases of aerodynamic shape optimization demonstrates the benefits and impacts of various design variables and constraints. As one would expect, the optimized BWB has the lowest drag coefficient when only lift and geometric constraints are enforced. However, this case also has a higher root bending moment and pitch moment than the baseline BWB. By adding trim and root bending moment constraints, the optimized drag coefficient increases by 14 counts relative to Case 1. The impact on the aerodynamic performance is mainly due to a less ideal spanwise lift distribution and increased drag from the reflex centerbody airfoil. We further explore the design space by adding span and sweep design variables to the optimization. The additional degrees-of-freedom provide about 4 drag count of improvement. This reduction comes from a lower skin friction drag and wave drag. Finally, we add both static margin constraint and CG design variable to the problem. We relax the CG location to allow the optimized BWB to meet the static margin

			Constraints				
C_D	Reduction	Design Variables	Geometric	Lift	Bending moment	Trim	Static margin
0.02696		Baseline	•	•			
0.02245	16.7%	Shape	•	•	•		
0.02381	11.7%	Shape	•	•	•	•	
0.02338	13.3%	Shape, Planform	•	•	•	•	
0.02339	13.2%	Shape, Planform, CG	•	•	•	•	•

Table 8. Summary of optimal drag coefficients, design variables, and constraints of the aerodynamic shape optimization cases

constraint without a large impact on the aerodynamic performance. The optimized configuration has less sweep than the previous case, which is limited by the static margin constraint. Allowing the CG location to move improves the performance: the CG is shifted aft to reduce the reflex on the centerbody and the downwash on the wing tip. The optimized BWB maintains the same drag coefficient as the case without static margin. Table 8 summarizes the four aerodynamic shape optimization cases.

V. Conclusion

In this work, we performed aerodynamic shape and planform optimization of a blended-wing-body aircraft using 800 shape design variables. We explored the effects of adding planform design variables. The sweep and span design variable provided 4 drag count of improvement at the cruise flight condition. We also investigated the degradation in aerodynamic performance due to the addition of root bending moment, trim, and static margin constraints. With the addition of a root bending moment constraint, the spanwise lift distribution on the optimized BWB departed from the elliptical lift distribution by shifting more loading inboard. The trim constraint resulted in an additional down twist to the wingtip, and it also added reflex to the rear of the centerbody airfoils. The static margin constraint limited the increase in sweep. The static margin was reduced to the lower bound by an aft CG location, which benefited the trim condition. We achieved an optimized BWB that is both trimmed and longitudinally stable, while reducing the drag by 13.2% compared to the baseline.

VI. Acknowledgements

The authors would like to thank Gaetan Kenway and Charles Mader for their assistance in various stages of this project. This work was funded by Michigan/AFRL/Boeing Collaborative Center in Aeronautical Sciences (MAB-CCAS). The computations were performed on high performance computing clusters in the Center for Advanced Computing at the University of Michigan, partially funded by University of Michigan College of Engineering.

References

[1] Jameson, A. and Ou, K., "50 Years of Transonic Aircraft Design," *Progress in Aerospace Sciences*, Vol. 47, No. 5, 2011, pp. 308–318. doi:10.1016/j.paerosci.2011.01.001.

[2] Liem, R. P., Kenway, G. K. W., and Martins, J. R. R. A., "Multi-Point, Multi-Mission, High-Fidelity Aerostructural Optimization of a Long-Range Aircraft Configuration," *14th AIAA/ISSMO Multidisciplinary Analysis and Optimization Conference*, Indianapolis, IN, September 2012, AIAA 2012-5706.

[3] Guynn, M., Berton, J., Fisher, K., Haller, W., Tong, M., and Thurman, D., "Engine Concept Study for an Advanced Single-Aisle Transport," *NASA TM-2009-215784*, 2009.

[4] Ryerson, M., Hansen, M., and Bonn, J., "Fuel Consumption and Operational Performance," *Transportation Research Part D*, Vol. 15, 2010, pp. 305–314.

[5] Hughes, K., Wu, C., Lamp, J., Coleman, A., Adili, P., Dhanoya, S., and White, K., "Optimizing Airport Arrival Operations: A Systems Engineering Analysis of Washington Dulles International Airport," *Systems and Information Design Symposium (SIEDS), 2012 IEEE*, IEEE, 2012, pp. 145–149. doi:10.1109/SIEDS.2012.6215139.

[6] Liebeck, R., "Design of the Blended Wing Body Subsonic Transport," *Journal of Aircraft*, Vol. 41, No. 1, 2004, pp. 10–25. doi:0.2514/1.9084.

[7] Kroo, I., "Innovations in Aeronautics," *42nd AIAA Aerospace Sciences Meeting, 5-8 January 2004, Reno, NV*, Vol. 4, 2004, pp. 1–11, AIAA 2004-0001.

[8] Qin, N., Vavalle, A., Le Moigne, A., Laban, M., Hackett, K., and Weinerfelt, P., "Aerodynamic Considerations of Blended Wing Body Aircraft," *Progress in Aerospace Sciences*, Vol. 40, No. 6, 2004, pp. 321–343. doi:10.1016/j.paerosci.2004.08.001.

[9] Stout, W., "A Low-A/R, All-Wing Light Plane with Pilot and Engine within Wing," Feb 1919, British Patent 149,708.

[10] Klemin, A., "Junkers"G-38", Progress of the Year, and more," *Scientific American*, Vol. 142, 1930, pp. 150–153. doi:10.1038/scientificamerican0230-150.

[11] Gunston, B., *Giants of the sky: the biggest aeroplanes of all time*, Haynes Pubns, October 1991.

[12] Risch, T., Cosentino, G., Regan, C., Kisska, M., and Princen, N., "X-48 B Flight-Test Progress Overview," *47th AIAA Aerospace Sciences Meeting Including the New Horizons Forum and Aerospace Exposition*, January 2009, AIAA 2009-2407.

[13] Callaghan, J. and Liebeck, R., "Some Thoughts on the Design of Subsonic Transport Aircraft for the 21st Century," *Aerospace Technology Conference and Exposition, October 1, 1990, Long Beach, California, United States*, 1990, pp. 5–13. doi:10.4271/901987, SAE Technical Paper 901987.

[14] Liebeck, R., Page, M., and Rawdon, B., "Evolution of the Revolutionary Blended-Wing-Body," *McDonnell-Douglas Aerospace, Transportation Beyond 2000: Technologies Needed for Engineering Design p 431-459*, 1996.

[15] Liebeck, R., Page, M., and Rawdon, B., "Blended-wing-body subsonic commercial transport," *36th AIAA Aerospace Sciences Meeting and Exhibit, 1998*, January 1998, AIAA 1998-0438.

[16] Potsdamt, M., Page, M., and Liebeck, R., "Blended wing body analysis and design," 1997, AIAA 1997-31774.

[17] Mukhopadhyay, V., Sobieszczanski-Sobieski, J., Kosaka, I., Quinn, G., and Vanderplaats, G., "Analysis, Design, and Optimization of Noncylindrical Fuselage for Blended-Wing-Body Vehicle," *Journal of Aircraft*, Vol. 41, No. 4, 2004, pp. 925–930. doi:10.2514/1.417.

[18] Liebeck, R., "Blended Wing Body Design Challenges," *Proceedings of AIAA International Air and Space Symposium and Exposition: The Next 100 Years, Dayton, Ohio*, 2003.

[19] Velicki, A., Thrash, P., and Jegley, D., "Airframe Development for the Hybrid Wing Body Aircraft," *47th AIAA Aerospace Sciences Meeting, Orlando, Florida*, January 2009, AIAA 2009-0932.

[20] Diedrich, A., Hileman, J., Tan, D., Willcox, K., and Spakovszky, Z., "Multidisciplinary design and optimization of the silent aircraft," *44th AIAA Aerospace Sciences Meeting*, January 2006, AIAA 2006-1323.

[21] Diedrich, A., *The Multidisciplinary Design and Optimization of an Unconventional, Extremely Quiet Transport Aircraft*, Ph.D. thesis, Massachusetts Institute of Technology, 2005.

[22] Wakayama, S., "Blended-wing-body optimization problem setup," *8th AIAA/ISSMO Symosium on Multidisciplinary Analysis and Optimization, Long Beach, CA*, September 2000, AIAA 2000-4740.

[23] Hileman, J., Spakovszky, Z., Drela, M., and Sargeant, M., "Airframe Design for Silent Aircraft," *45th AIAA Aerospace Sciences Meeting and Exhibit, Reno, Nevada*, January 2007, AIAA 2007-0453.

[24] Meheut, M., Grenon, R., Carrier, G., Defos, M., and Duffau, M., "Aerodynamic Design of Transonic Flying Wing Configurations," *KATnet II: Conference on Key Aerodynamic Technologies, Bremen, Germany*, 2009.

[25] Mialon, B., Fol, T., and Bonnaud, C., "Aerodynamic Optimization of Subsonic Flying Wing Configurations," *20th AIAA Applied Aerodynamics Conference, St. Louis, MO*, June 2002, AIAA 2002-2931.

[26] Mialon, B. and Hepperle, M., "Flying Wing Aerodynamics Studies at ONERA and DLR," *MH*, Vol. 150, 2005, pp. 3.

[27] Strüber, H. and Hepperle, M., "Aerodynamic Optimisation of a Flying Wing Transport Aircraft," *New Results in Numerical and Experimental Fluid Mechanics V*, 2006, pp. 69–76.

[28] Denisov, V., Bolsunovsky, A., Buzoverya, N., and Gurevich, B., "Recent Investigations of the Very Large Passenger Blended-Wing-Body Aircraft," *Proceedings of ICAS*, 1998, ICAS 98-4102.

[29] Bolsunovsky, A., Buzoverya, N., Gurevich, B., Denisov, V., Shkadov, L., and Udzhukhu, A., "Investigations on Possible Characteristics of FW Superhigh Seating Capacity Airplane," *Proceedings 22st ICAS Congress*, 2000.

[30] Bolsunovsky, A., Buzoverya, N., Gurevich, B., Denisov, V., Dunaevsky, A., Shkadov, L., Sonin, O., Udzhuhu, A., and Zhurihin, J., "Flying wing–problems and decisions," *Aircraft design*, Vol. 4, No. 4, 2001, pp. 193–219. doi:10.1016/S1369-8869(01)00005-2.

[31] Morris, A., "The MOB Project: Towards Methods to Support E-Design Across Europe," *Air & Space Europe*, Vol. 3, No. 3-4, 2001, pp. 73–79. doi:10.1016/S1290-0958(01)90061-9.

[32] Morris, A., "MOB a European Distributed Multi-disciplinary Design and Optimisation Project," *Proceedings of the 9th AIAA/ISSMO Symposium on MDO*, September 2002, AIAA 2002-5444.

[33] Morris, A., Arendsen, P., LaRocca, G., Laban, M., Voss, R., and Hönlinger, H., "Mob - A European Project on Multidisciplinary Design Optimisation," *24th ICAS Congress*, 2004.

[34] La Rocca, G., Krakers, L., and van Tooren, M., "Development of an ICAD Generative Mmodel for Blended Wing Body Aircraft Design," *9th AIAA/ISSMO Symposium on Multidisciplinary Analysis and Optimization*, September 2002, AIAA 2002-5447.

[35] Laban, M., Arendsen, P., Rouwhorst, W., and Vankan, W., "A Computational Design Engine for Multi-disciplinary Optimisation with Application to a Blended Wing body Configuration," *9 th AIAA/ISSMO Symposium and Exhibit on Multidisciplinary Analysis and Optimization, Atlanta, GA*, September 2002, AIAA 2002-5446.

[36] Qin, N., Vavalle, A., Le Moigne, A., Laban, M., Hackett, K., and Weinerfelt, P., "Aerodynamic studies of blended wing body aircraft," *9 th AIAA/ISSMO Symposium and Exhibit on Multidisciplinary Analysis and Optimization, Atlanta, GA*, September 2002, AIAA 2002-5448.

[37] Qin, N., Vavalle, A., and Le Moigne, A., "Spanwise Lift Distribution for Blended Wing Body Aircraft," *Journal of aircraft*, Vol. 42, No. 2, 2005, pp. 356–365. doi:10.2514/1.4229.

[38] Roman, D., Gilmore, R., and Wakayama, S., "Aerodynamics of High-subsonic Blended-Wing-Body Configurations," *41st Aerospace Sciences Meeting and Exhibit, Reno, NV*.

[39] Kuntawala, N., Hicken, J., and Zingg, D., "Preliminary Aerodynamic Shape Optimization Of A Blended-Wing-Body Aircraft Configuration," *49th AIAA Aerospace Sciences Meeting, Orlando, Florida*, January 2011, AIAA 2011-0642.

[40] Kuntawala, N., *Aerodynamic Shape Optimization of a Blended-Wing-Body Aircraft Configuration*, Ph.D. thesis, University of Toronto, 2011.

[41] Mader, C. A. and Martins, J. R. R. A., "Stability-Constrained Aerodynamic Shape Optimization of Flying Wings," *Journal of Aircraft*, 2012, (In press).

[42] Mader, C. A., Martins, J. R. R. A., Alonso, J. J., and van der Weide, E., "ADjoint: An Approach for the Rapid Development of Discrete Adjoint Solvers," *AIAA Journal*, Vol. 46, No. 4, April 2008, pp. 863–873. doi:10.2514/1.29123.

[43] Kenway, G. K. W., Kennedy, G. J., and Martins, J. R. R. A., "A CAD-Free Approach to High-Fidelity Aerostructural Optimization," *Proceedings of the 13th AIAA/ISSMO Multidisciplinary Analysis Optimization Conference*, Fort Worth, TX, September 2010, AIAA 2010-9231.

[44] Kenway, G. K. W., Kennedy, G. J., and Martins, J. R. R. A., "A scalable parallel approach for high-fidelity steady-state aeroelastic analysis and derivative computations," *AIAA Journal*, 2012, (Accepted subject to revisions) http://mdolab.engin.umich.edu/content/scalable-parallel-approach-aeroelastic-analysis-and-derivative.

[45] Sederberg, T. and Parry, S., "Free-form Deformation of Solid Geometric Models," *ACM Siggraph Computer Graphics*, Vol. 20, ACM, 1986, pp. 151–160. doi:10.1145/15886.15903.

[46] van der Weide, E., Kalitzin, G., Schluter, J., and Alonso, J. J., "Unsteady Turbomachinery Computations Using Massively Parallel Platforms," *Proceedings of the 44th AIAA Aerospace Sciences Meeting and Exhibit*, Reno, NV, 2006, AIAA 2006-0421.

[47] Kenway, G. K. W. and Martins, J. R. R. A., "Multi-point High-Fidelity Aerostructural Optimization of a Transport Aircraft Configuration," *Journal of Aircraft*, 2012, (Submitted) http://mdolab.engin.umich.edu/content/multi-point-aerostructural-optimization-transport-aircraft-configuration.

[48] Martins, J. R. R. A., Alonso, J. J., and Reuther, J. J., "High-Fidelity Aerostructural Design Optimization of a Supersonic Business Jet," *Journal of Aircraft*, Vol. 41, No. 3, 2004, pp. 523–530. doi:10.2514/1.11478.

[49] Saad, Y. and Schultz, M., "GMRES: A Generalized Minimal Residual Algorithm for Solving Nonsymmetric Linear Systems," *SIAM Journal on scientific and statistical computing*, Vol. 7, No. 3, 1986, pp. 856–869. doi:10.1137/0907058.

[50] Martins, J. R. R. A., Alonso, J. J., and Reuther, J. J., "A Coupled-Adjoint Sensitivity Analysis Method for High-Fidelity Aero-Structural Design," *Optimization and Engineering*, Vol. 6, No. 1, March 2005, pp. 33–62. doi:10.1023/B:OPTE.0000048536.47956.62.

[51] Dixon, L. and Mills, D., "Effect of rounding errors on the variable metric method," *Journal of optimization theory and applications*, Vol. 80, No. 1, 1994, pp. 175–179. doi:10.1007/BF02196600.

[52] Perez, R. E., Jansen, P. W., and Martins, J. R. R. A., "pyOpt: A Python-Based Object-Oriented Framework for Nonlinear Constrained Optimization," *Structures and Multidisciplinary Optimization*, Vol. 45, No. 1, 2012, pp. 101–118. doi:10.1007/s00158-011-0666-3.

[53] Gill, P. E., Murray, W., and Saunders, M. A., "SNOPT: An SQP Algorithm for Large-Scale Constrained Optimization," *SIAM Review*, Vol. 47, No. 1, 2005, pp. 99–131. doi:10.1137/S0036144504446096.

[54] Lee, D. and Faget, M., "Charts Adapted from Van Driest's Turbulent Flat-Plate Theory for Determining Values of Turbulent Aerodynamic Friction and Heat-Transfer Coefficients," 1956, NACA TN 3811.

[55] Martins, J. R. R. A. and Lambe, A. B., "Multidisciplinary design optimization: A Survey of architectures," *AIAA Journal*, 2012, (In press) http://mdolab.engin.umich.edu/content/multidisciplinary-design-optimization-survey-architectures-1.

[56] Jones, R., "The Spanwise Distribution of Lift for Minimum Induced Drag of Wings Having a Given Lift and a Given Bending Moment," *NASA Tech. Report*, 1950, NACA-TN-2249.

[57] Stinton, D., *The design of the airplane*, American Institute of Aeronautics and Astronautics and Blackwell Science, UK, 2001.

[58] CAC, "CAEN Advanced Computing, the University of Michigan," December 2012, http://cac.engin.umich.edu/.

[59] Kroo, I., "Drag due to Lift: Concepts for Prediction and Reduction," *Annual Review of Fluid Mechanics*, Vol. 33, No. 1, 2001, pp. 587–617. doi:10.1146/annurev.fluid.33.1.587.

[60] Gyorgyfalvy, D., "Performance analysis of the Horten IV flying wing," *8th Congress of the Organisation Scientifique et Technique Internationale due Vol a Vile, Cologne, Germany*, June 1960.

[61] Maratos, N., *Exact Penalty Function Algorithms for Finite Dimensional and Control Optimization Problems*, Ph.D. thesis, Imperial College London (University of London), 1978.